

Orientation discrimination of single-stranded DNA inside the α -hemolysin membrane channel

Jérôme Mathé*, Aleksei Aksimentiev†, David R. Nelson‡, Klaus Schulten†, and Amit Meller*§

*Rowland Institute, Harvard University, Cambridge, MA 02142; †Beckmann Institute, University of Illinois, Urbana, IL 61801; and ‡Lyman Laboratory of Physics, Harvard University, Cambridge, MA 02138

Edited by Stephen L. Mayo, California Institute of Technology, Pasadena, CA, and approved July 12, 2005 (received for review April 11, 2005)

We characterize the voltage-driven motion and the free motion of single-stranded DNA (ssDNA) molecules captured inside the ≈ 1.5 -nm α -hemolysin pore, and show that the DNA–channel interactions depend strongly on the orientation of the ssDNA molecules with respect to the pore. Remarkably, the voltage-free diffusion of the 3'-threaded DNA (in the trans to cis direction) is two times slower than the corresponding 5'-threaded DNA having the same poly(dA) sequence. Moreover, the ion currents flowing through the blocked pore with either a 3'-threaded DNA or 5' DNA differ by $\approx 30\%$. All-atom molecular dynamics simulations of our system reveal a microscopic mechanism for the asymmetric behavior. In a confining pore, the ssDNA straightens and its bases tilt toward the 5' end, assuming an asymmetric conformation. As a result, the bases of a 5'-threaded DNA experience larger effective friction and forced reorientation that favors co-passing of ions. Our results imply that the translocation process through a narrow pore is more complicated than previously believed and involves base tilting and stretching of ssDNA molecules inside the confining pore.

asymmetry | DNA translocation | DNA hairpin

The transport of biomolecules across cell walls is a ubiquitous process in biology, controlled by membrane proteins that act as selective channels and transporters (1, 2). These processes usually involve the passage of a biopolymer through a narrow proteinic confinement that, in the case of polynucleic acids, can result in temporary structural deformations of the molecules. The ability of membrane proteins to sort single molecules, and in particular polynucleic acids, is also of great interest in bioengineering. In the past few years membrane channels like the bacterial α -hemolysin (α -HL) have been adapted as *in vitro* devices for rapid, single-molecule nucleic acid characterization (3–7). In these experiments the negatively charged single-stranded DNA (ssDNA) or RNA molecules were electrophoretically driven through a single, membrane-embedded pore having dimensions that are only slightly larger than the size of a nucleotide (8). The passage time of each individual molecule was measured by monitoring the residual ion current flowing through the pore during the transport of the biopolymer. One of the important findings has been that the translocation dynamics is dominated by the nucleic acid interactions with the pore walls, and that these interactions are substantially stronger for purine-rich DNA sequences as compared with pyrimidine-rich molecules (5, 9). However, the microscopic source for this sequence selectivity as well as the exact shape of the interaction potential between the DNA and the pore have not yet been resolved. In particular, it was unclear whether the asymmetric structure of α -HL (8) coupled with the directionality of ssDNA can lead to asymmetric polynucleotide dynamics, with and without an external biasing potential.

To address these questions, we have carried out extensive DNA translocation experiments, which take advantage of the finding that ssDNA can enter the trans membrane pore of the α -HL, but double-stranded DNA cannot (8, 10–12). Thus, DNA hairpin molecules with a long single-stranded overhang only enter the α -HL pore with the single-stranded part, either the 3'

or the 5' end, depending on the DNA construct. As a result, the blockade currents and the DNA transport resulting from either 3' or 5' entries can be unambiguously discriminated and characterized. Moreover, by taking advantage of the dynamic voltage control method (13), the escape dynamics of molecules from the pore can be measured at a finite voltage level, as well as at $V = 0$. Previous DNA translocation experiments have revealed two peaks in the translocation time distribution (3) as well as in the blockade current histogram (5, 7, 13) comprised of several hundred translocation events from identical molecules. The two peaks have been associated with the direction of polynucleotide translocation, either 3' or 5' end first (5, 7, 14). However, it remained unclear which of the two orientations produce the shorter blockade times and the lower blockade current. Here, we show that 3' end DNA entries induce a larger current blockade as compared with the 5' end threading, and measure the fundamental, voltage-free diffusion constants associated with either 3' or 5' threading of ssDNA through the pore. Remarkably, we found that the voltage-free dynamics of the 3'-threaded molecules (entering and exiting from the same side of the pore) is two times slower than the corresponding diffusion of the 5' threading.

To delineate the underlying mechanism responsible for the observed dynamics, we carried out all-atom molecular dynamics (MD) simulations, using the known structures of the α -HL pore and the DNA. The MD simulations independently confirmed the experimental results, indicating that the 3' threading blocks the ion current more effectively and will result in stronger interactions. Moreover, the MD data allow us to pinpoint a mechanistic explanation for the observed asymmetry in DNA dynamics based on a microscopic picture. We find that the confinement of the ssDNA in the α -HL pore results in straightening of the DNA backbone and, consequently, in a collective tilt of the bases with respect to the DNA backbone in the direction of the 5' end of the molecule, and that this tilt can create an asymmetric DNA–pore interaction. Noteworthy is the fact that the MD simulations were performed without any *a priori* knowledge of the experimental data (i.e., which orientation is faster or causes larger ion current blockade). Our results agree with a theoretical model that describes the DNA–pore interactions by using a different asymmetric sawtooth potential for each orientation (14). These potentials yield asymmetric dynamics of the threaded DNA even at zero applied voltage, as observed in our experiments.

Methods

Experiments. PAGE-purified ssDNA and DNA hairpins (Eurogentec, San Diego) were buffered in 10 mM Tris/1 mM EDTA (pH 8.5) solution. Before each measurement the samples were heated to 75°C for 10 min and then quenched to 4°C. The hairpins are constituted of a single-stranded overhang of 50

This paper was submitted directly (Track II) to the PNAS office.

Abbreviations: α -HL, α -hemolysin; MD, molecular dynamics; ssDNA, single-stranded DNA.

§To whom correspondence should be addressed. E-mail: meller@rowland.harvard.edu.

© 2005 by The National Academy of Sciences of the USA

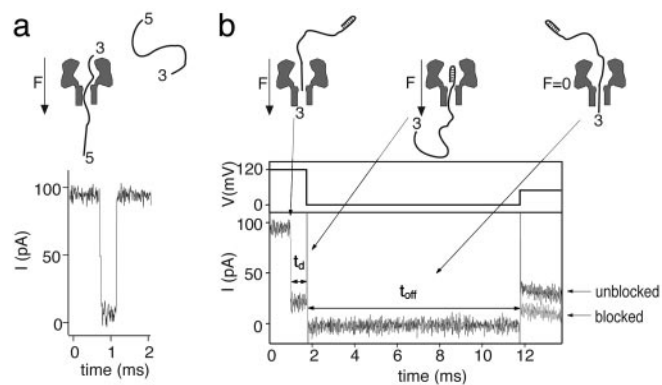


Fig. 1. DNA hairpins can be used to facilitate translocation and diffusion measurements as a function of their orientation. (a) With ssDNA, 3' and 5' entries to the nanopore are mixed. (Inset) A typical translocation event measured with $V = 120$ mV. (b) The escape probability of DNA hairpins, with long single-stranded overhang, can be measured as a function of t_{off} by using dynamic voltage control (see text). (Inset) The applied voltage and the corresponding current traces for two events. Note that at the end of the t_{off} period only one of two options can exist: an empty pore or a blocked pore, either of which are readily detected by applying a small probing voltage (13).

adenines and a 10-bp double-stranded part closed by a loop of 6 bases, with the following sequences: HP3', 5'-GCTCTGTT-GCTCTCTCGCAACAGAGC(A)₅₀; HP5', 5'-(A)₅₀CGAGACA-ACGCTCTCTCGTTGTCTCG. Notice that the two sequences are the same except for the writing direction. Because the α -HL cannot admit double-stranded parts into its β -barrel, the molecule can only enter by its overhang part: 3' end for HP3' and 5' end for HP5'.

The basic apparatus and experimental method for reconstituting the α -HL channel in a horizontally supported planar bilayer are described in ref. 15. The temperature of our system was maintained at $15.0 \pm 0.1^\circ\text{C}$ by using a custom cell design (13). The two chambers of the cell (cis and trans) were filled with a 1 M KCl/10 mM Tris-Cl buffer with a pH of 8.5, and voltage was applied across the bilayer by using two Ag/AgCl electrodes connected to a patch clamp headstage. The ground electrode was connected to the cis side. The current signal was filtered by using a 100-kHz low-pass 4-poles Butterworth filter and was digitized at 1 MHz/12 bits. Our acquisition system included a dynamic control of the voltage to apply any pattern of voltage after the entry of each DNA molecule in the pore (12, 13). This feature is particularly useful for studying low-voltage dynamics of DNA in the pore.

In the experiments presented, we measured the ion current flowing through the pore containing DNA hairpin molecules, which were threaded to the pore from the cis chamber with either their 3' end (HP3') or the 5' end (HP5') as shown in Fig. 1b. For both hairpin molecules, we also measured the dynamics of entry and exit from the cis side of the pore. These experiments were performed by using the following procedure: the voltage was first set to 120 mV to draw the DNA molecules into the pore, probed by an abrupt blockade of the ionic current of $\approx 90\%$, the molecules were further pulled in for a fixed driving time, t_d , at 120 mV. Then the voltage was set to zero for a period of waiting time t_{off} , and finally a small positive probing voltage V_p was applied to probe whether the molecules stayed in the pore during the "off" period or not. This procedure was fully automated and computer-controlled (12). By repeating each measurement over 1,500 times, we can establish the probability to find a molecule in the pore, P_{stay} , at each given waiting time. In some experiments

t_{off} was set to zero, and V_p was set to negative values to measure the translocation driven in the reverse direction.

Simulations. All MD simulations were performed by using the program NAMD (16). The phantom pore simulations (described below) comprising water, ions, and DNA were carried out by using the AMBER95 (17) force field. The CHARMM27 (18) force field was deployed for all other simulations, which include water, ions, DNA, protein, and lipids. The temperature was kept at 288 K by applying Langevin forces; other simulation conditions and protocols are described in ref. 19. A 58-bp double-stranded DNA helix was built from individual base pairs in the geometry suggested by QUANTA (Polygen, Waltham, MA). Single-stranded DNA was obtained from that structure by removing one of the strands. The remaining strand was then solvated in a preequilibrated volume of TIP3P water molecules; K^+ and Cl^- ions were added, corresponding to a 1 M concentration. The resulting system was equilibrated for 12 ns. The poly(dA)₅₈ strand was constructed from the equilibrated DNA strand by replacing all non-adenine DNA bases with adenine.

An all-atom model of the α -HL channel assembled with a lipid bilayer was constructed, simulated, and tested extensively as described in ref. 19. To thread a DNA strand through the α -HL pore, KCl electrolyte was built around a DNA strand, conforming to the shape of the α -HL pore; the pore profile, which is not a cylinder, was determined from a 50-ns MD simulations of α -HL in lipid bilayer as shown in figure 4a of ref. 19. The shape of the α -HL pore was represented by a mathematical surface, which we call here a phantom pore. Initially, the phantom pore was made 2 nm wider in diameter than the pore of α -HL, so that the entire 58-nt strand could fit into it. The pore was then gradually shrunk in a 2-ns simulation to its original shape (the shape of the α -HL pore). At the same time, 10-pN forces pushed all atoms laying outside of the shrinking surface toward the center of the pore. At the end of the simulation, the DNA strand adapted a straight conformation that conformed to the shape of the α -HL pore. We carried out two such simulations (in the NpT ensemble) corresponding to the two global orientations of the DNA strand inside the pore. Each DNA strand, as well as the ions found in the stem region of the phantom pore, were merged with the all-atom model of the α -HL channel. In the resulting structure, water, and ions covered the DNA strand completely; one such system is shown in Fig. 7b. After 2,000 steps of minimization with all DNA atoms fixed, each system was equilibrated for 2 ns in the NpT ensemble.

Results

Experiments. We characterize the translocation time and current, which correspond to the passage of a single DNA molecule from the cis side of the pore to the trans side, by the time period and mean current during which the current is blocked by $>75\%$ (t_T and I_b , respectively, as defined in ref. 5). Fig. 2a is a histogram of the normalized I_b values measured from $\approx 2,000$ events similar to the one shown in Fig. 1a, for a 60-mer poly(dA) ssDNA. The current histogram exhibits two well defined populations and was fit by a double Gaussian distribution. The primary and secondary peaks are centered on normalized currents of 0.09 and of 0.12, respectively. Although the source of the double peak is not obvious, it had been previously proposed that DNA entry on either the 3' or the 5' is responsible for the two blockade currents peaks (5, 7, 14). If this is the case, the area under each Gaussian in Fig. 2a indicates that the translocation of the DNA in one of the orientation is preferred over the other orientation. However, this experiment cannot tell us which end is privileged.

To delineate the source of the two peaks in Fig. 2a, we measured the mean current during the driving time (t_d) of the single-stranded overhang in hairpins HP3' and HP5' (see *Methods*). The resulting current histograms are overlaid in Fig. 2b

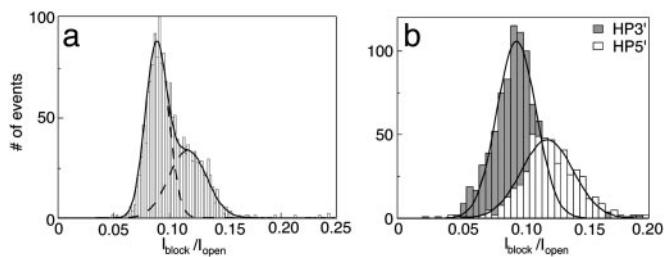


Fig. 2. Comparison between the distributions of the blocked ion current from ssDNA and ssDNA with terminal hairpins, threaded into the α -HL pore. (a) Mean translocation current distribution for a ssDNA [poly(dA₆₀)]. Although the solution contains only one, monodispersed population of DNA molecules, the current distribution displays two peaks, a primary peak at 0.09 and a minor peak at 0.12. (b) Histogram of mean blockade current for DNA hairpin HP3' (gray bars) and HP5' (white bars). The curves are Gaussian fits yielding peak values of 0.09 ± 0.02 and 0.12 ± 0.03 for HP3' and HP5', respectively. Data were accumulated for the same fixed period for the two hairpins, under identical conditions. In these distributions, each molecule was counted once.

(HP3' in gray and HP5' in white). In this experiment, we accumulated data (for each hairpin type) for a fixed period. The concentration of the hairpins in the two measurements were identical. Note that, for each hairpin, we detected a single peak, which can be closely approximated by a Gaussian. From the fits, we found that the peak corresponding to HP3' is at 0.09 ± 0.02 and the one corresponding to HP5' is at 0.12 ± 0.03 . These numbers are in excellent agreement with the values of the two peaks found in the translocation current histogram of the single-stranded poly(dA) described earlier. Moreover, note that the ratio of the amplitudes of the two Gaussians in Fig. 2*b* are very close to the corresponding amplitudes of the double Gaussian fit shown in Fig. 2*a*. Given that the two hairpin experiments were performed under identical conditions (in both cases data were accumulated for 30 min by using the same DNA concentration), it is clear that (i) the 3' end on the DNA is more likely to enter from the cis side of the pore as compared with the 5' end, (ii) the source for the two peaks in Fig. 2*a* is most likely the two possible DNA orientations, and (iii) the 3' entries give rise to a larger blockade in the current (smaller residual current).

To further elucidate the dependence of the DNA–pore interactions on the orientation of the polynucleotides inside the pore, we have performed a variety of dynamic measurements, to characterize the translocation time and escape probability (as a function of time) of HP3' and HP5' in the nanopore. In the first experiment, we took advantage of the large gap in the most probable translocation time, t_p , of the poly(dA₅₀) and the typical unzipping time of the 10 bases hairpin at 120 mV (280 and 2,000 μ s, respectively) (12, 13) (see supporting information, which is published on the PNAS web site), to measure the escape probability at $V = 0$ for HP3' and HP5', under the same initial conditions. We chose a value for t_d of 750 μ s, which is much longer than the typical translocation time and much smaller than the typical unzipping time, and performed diffusion measurements as described in *Methods* (see Fig. 1*b*).

The probabilities that a molecule will stay in the pore, P_{stay} , as a function of the waiting time, t_{off} , are displayed in Fig. 3 in a semi log plot. Notice that, at the very short times ($t < 100 \mu$ s), some molecules rapidly escape from the pore with a characteristic time scale of $\approx 50 \mu$ s. This process is too fast to be accurately probed by our experimental setup mainly because of the dead time in the ion current measurement immediately after the abrupt switching to zero voltage. In contrast, the long time regime ($t > 100 \mu$ s) can be well approximated by monoexponential functions (solid lines), over ≈ 3 decades in time, with characteristic times (amplitudes) of 15,000 μ s (0.78) and 8,800 μ s (0.32) for HP3' and

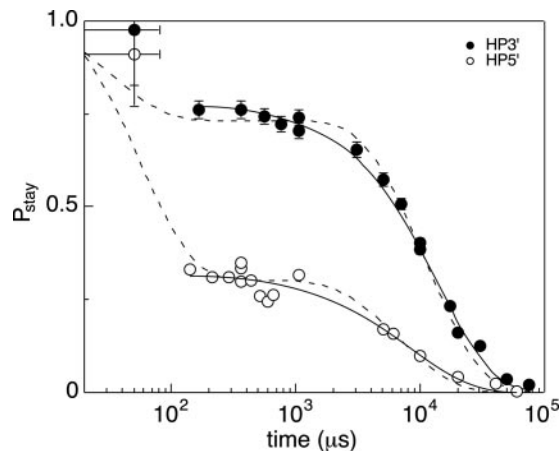


Fig. 3. The probability that a molecule will stay in the pore, P_{stay} , as a function of the waiting time, t_{off} , after threading of the single-stranded overhang into the pore ($t_d = 750 \mu$ s) for HP3' molecules (filled symbols) and HP5' (open symbols). Solid lines represent monoexponential fits to the data at $t > 100 \mu$ s. Dashed lines are fits to the data according to the model discussed in the text. Each data point in this graph is a compilation of nearly 1,500 events (over 60,000 molecules were individually analyzed for this graph).

HP5', respectively. The amplitudes of these fits are mainly determined by the fraction of molecules that escape from the pore in the early times ($t < 100 \mu$ s). However, because the amplitude associated with HP3' is much larger than the one associated with the HP5', it is clear that more HP3' molecules remained in the pore after 100 μ s than HP5'. More striking is the fact that the characteristic escape time of the HP3' is 1.70 times longer than that of the HP5' (15,000 μ s/8,800 μ s = 1.70). This result is surprising given that the sequence, the length, and the initial conditions in the two experiments are identical. We can also rule out that interactions of the hairpin portion with the α -HL vestibule are a significant contributor for the differences between the two curves for the following reasons: (i) As shown in Fig. 4, changing the initial threading times of the single-stranded overhangs resulted in a marked shift of the P_{stay} curves for the two hairpins; and (ii) in other experiments, we have verified that P_{stay} is highly sensitive to the length and the sequence of the single-stranded overhangs, and not to the stem part (M. Bates and A.M., unpublished work). Thus, it is very likely that the escape dynamics is dominated by the interactions of the single-stranded portion of the DNA with the pore, and that the remarkable difference between the two hairpins is due to the different orientations of the polynucleotides in the two cases.

To validate our assumption that in the early times some molecules can quickly escape from the pore, we performed

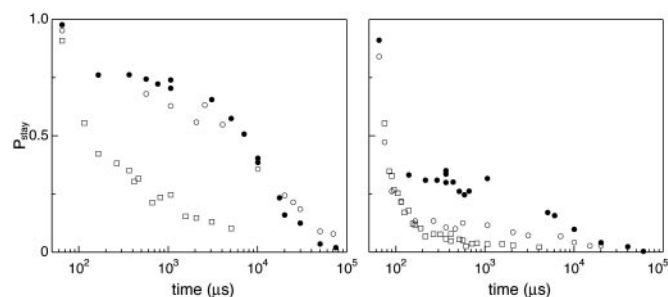


Fig. 4. P_{stay} of each hairpin as a function of the driving time in the pore. (Left) HP3'. (Right) HP5'. Filled circles, $t_d = 750 \mu$ s; open circles, $t_d = 300 \mu$ s; squares, $t_d = 100 \mu$ s. Each data point in the graphs is a compilation of nearly 1,500 separate molecules.

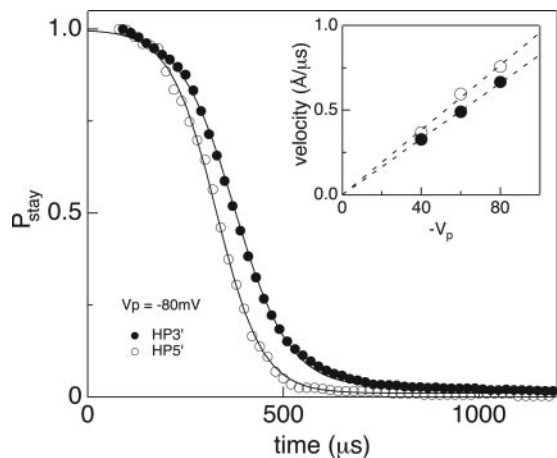


Fig. 5. Measured probability distributions of staying in the pore of the fully threaded hairpins after a negative voltage V_p is applied, as a function of time. Results for HP3' (filled circles) and HP5' (open circles) are shown in the main figure for $V_p = -80$ mV. (Inset) The characteristic escape velocity measured as a function of V_p (see text). The escape velocity is higher for the HP5' molecules as compared with the HP3' for all values of V_p by a factor of 1.16.

experiments with shorter t_d , i.e., times that are comparable or much shorter than the most probable translocation time ($t_P = 280 \mu\text{s}$). If our assumption is correct, we expect that using shorter driving times the fraction of the fast escaping molecules will grow, and that for $t_d < t_P$ the escape probability function will be much more complicated than the one discussed above, because it involves molecules that are threaded into the pore to varying degrees. This trend is indeed borne out by our data: In Fig. 4, we display the P_{stay} data obtained for three different driving times: $t_d = 100, 300,$ and $750 \mu\text{s}$. Fig. 4 *Left* corresponds to experiments with HP3', and Fig. 4 *Right* corresponds to experiments with HP5'. As expected, the probability to find a molecule in the pore increases, in general, for longer values of t_d , but there is a considerable difference between the two sets of curves. In the HP3' case the curves corresponding to $t_d = 300$ and $750 \mu\text{s}$ almost overlap, whereas $t_d = 100 \mu\text{s}$ stands out. This finding indicates that for HP3' most of the molecules were completely threaded for $t_d \geq 300 \mu\text{s}$. In addition, the data obtained with $t_d = 100 \mu\text{s}$ display complicated dynamics that cannot be approximated by using a single exponential function. In contrast, in the case of HP5' the curves corresponding to $t_d = 100 \mu\text{s}$ and $300 \mu\text{s}$ are similar, whereas the $750\text{-}\mu\text{s}$ curve is substantially higher. Thus, $300 \mu\text{s}$ was not long enough to completely thread the hairpins. Performing measurements with t_d longer than $t_d = 750 \mu\text{s}$ resulted in identical P_{stay} probabilities for the HP5' and HP3' (data not shown). This result is expected based on the fact that the translocation time probability for poly(dA₅₀) at 120 mV is essentially zero above $750 \mu\text{s}$ (see supporting information) (13). The overall trend in Figs. 3 and 4 indicates that the voltage-free diffusion of the hairpins from trans to cis is slower for HP3' than HP5', and that the voltage-driven sliding of 3' DNA molecules from cis to trans is faster than the sliding of the 5' end. Notice that this result is in line with the smaller amplitude of the exponential fits shown in Fig. 3.

In a third set of measurements, we probed the response of the two hairpin molecules to negative potentials, after completely threading them into the pore. The measurements were performed similarly to the diffusion experiments described above: The molecules were threaded into the pore by using $V_d = 120$ mV and $t_d = 750 \mu\text{s}$, then a negative voltage V_p was applied and the current was probed over a 20-ms period. Data were analyzed by calculating the fraction of molecules that stay in the pore after a given time t . Results for $V_p = -80$ mV are shown in Fig. 5 for

HP3' (filled circles) and for HP5' (open circles). The normalized probabilities decrease from 1 at short times to zero with a characteristic time scale, τ , obtained by fitting the curves to sigmoidal functions. We repeated the experiments for $V_p = -60$ mV and -40 mV. The characteristic velocities of the hairpins (obtained by the ratio L/τ , where L is the single-stranded length) are shown as a function of V_p in Fig. 5 *Inset*. Notice that in all cases the τ values associated with HP3' are longer than the corresponding times associated with HP5', with an average ratio $\tau_{\text{HP3'}/\tau_{\text{HP5'}}$ of 1.16 ± 0.05 . Thus, the escape of HP3' molecules in the trans-to-cis direction is slower than HP5' escape, consistent with the $V = 0$ results shown in Fig. 3. In addition, the ratio of characteristic escape times in the zero voltage case is higher than the one obtained at finite voltage.

Simulations. To reveal how the global orientation of a DNA strand determines its kinetic properties, as well as the blockade of ionic current, we examined in atomic detail conformations of DNA in solution and inside α -HL. Before running MD simulations, two identical poly(dA₂₀) strands, different only by their global orientation, were aligned with each other (see supporting information). The two strands appeared to have, overall, similar conformations, the only difference visible being the ordering of the backbone atoms: When moving along the strand from 5' to 3' end, a phosphate group follows the deoxyribose sugar ring, the C5' carbon of deoxyribose follows the phosphate. Reversing the order changes the orientation of deoxyribose in the backbone. Although this change is sufficient to disrupt the function of a dephosphorylative enzyme, when put into the perspective of the α -HL structure, it is an unlikely reason for the observed directionality. First, our experiments showed no evidence of a chemical reaction between α -HL and DNA; second, if one assumes that a DNA strand is mobile inside the α -HL pore (and our MD simulations confirm this assumption), 12 sugars forming the backbone of a DNA fragment confined within the α -HL pore should be able to sample the pore's interior regardless of the sugars' orientation.

Another possible explanation for the observed 3' and 5' directionality might be that an ensemble of DNA conformations, by itself, contains the information about the global orientation of a DNA strand. To determine whether this is the case, we computed the average angle between nucleotide bases and the backbone in a DNA strand submerged in water. Our results (see supporting information) indicate that for purine nucleotides (A and G) the most probable angle is $\approx 88^\circ$, whereas for pyrimidines (C and T) that angle is $\approx 105^\circ$. From this analysis, we conclude that local conformations can indeed indicate a global orientation preference of a DNA strand, although the conformational anisotropy in an unrestrained strand is small and depends on sequence.

To investigate the influence of the restricted pore geometry on the ensemble of conformations adapted by a DNA strand, a poly(dA₁₁) strand, submerged in a 1 M KCl solution, was confined by a mathematical surface representing the shape of a cylindrical pore. Initially, this pore was wide enough to accommodate the entire ssDNA strand the backbone of which assumed a Watson-Crick helical form. During a 1.2-ns simulation, the diameter of the pore was reduced from 3.0 to 1.0 nm. DNA atoms that lay outside of this surface were subject to a 10-pN force directed toward the center of the pore. These forces adjusted conformations of DNA to the shape of the pore with the DNA backbone straightened; water and ions were not subject to the restraining force in this simulation. In Fig. 6a, we plot the resulting average base-backbone angle as a function of the pore diameter. Similar results were obtained with poly(dC₁₁) and dC₇dAdC₃ strands. We noticed that when the pore becomes < 1.5 nm in diameter, the DNA bases of ssDNA start to tilt collectively toward the 5' end of the strand. DNA bases were observed to tilt

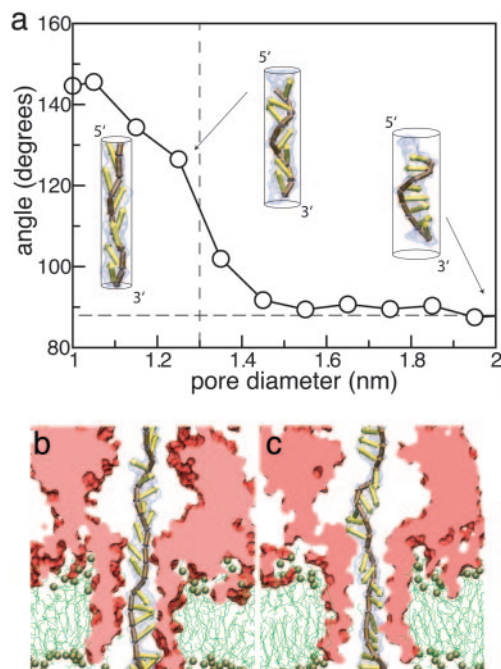


Fig. 6. Alignment of DNA bases in confined geometry. (a) The average angle between the base and the backbone of a nucleotide in a poly(dA₁₁) strand confined inside a cylindrical pore, from a 1.2-ns MD simulation. Snapshots (at 1.0, 1.25, and 3.0 nm, from left to right) illustrate DNA conformations during this simulation when the diameter of the pore was reduced from 3.0 to 1.0 nm. The horizontal dashed line indicates the most probable base–backbone angle in an unconstrained strand. Inside small pores (≤ 1.5 nm) the DNA bases are tilted toward the 5' end of the strand. The vertical dashed line at 1.3 nm corresponds to the narrow constriction in the α -HL. The tilt of the DNA bases inside the α -HL pore depends on the global orientation of the strand: In the (cis)5'-dA₅₈-3'(trans) strand (b) bases are tilted upward, whereas in the (cis)3'-dA₅₈-5'(trans) strand (c) bases are tilted downward.

toward the 5' end of the strand also when a 58-nt strand was confined inside a phantom pore shaped like the α -HL channel as shown in Fig. 6*b* and *c*. The same tilt was observed without confinement when the DNA backbone was stretched (see supporting information).

What consequence does the uniform tilting of the bases have on DNA translocation kinetics and on current blockades? Intuitively, one could equate driving ssDNA with an electric field through the narrow constriction of α -HL to bringing a tree through a door: The tree moves more easily trunk first than tip first (because branches tend to grow toward the tip of the tree). Naturally, to determine the molecular mechanism underlying DNA directionality, one has to visualize the translocation event in atomic detail. Currently available computer resources only allow MD simulations of a few tens of nanoseconds. However, one can start a simulation with the DNA strand threaded halfway through the pore and inspect over a few nanoseconds in how far switching on an electrical field drives the strand for the next few nanoseconds through the pore.

We have adopted this procedure to test the directionality dependence of the field-induced transport of ssDNA. Two systems, each comprising one α -HL channel, a DPPC membrane, a poly(dA₅₈) strand, water, and ions, were subject to an external electric field equivalent to a 1.2-V bias. In the first system, the 5' end of the strand was located at the trans side of the membrane. This orientation will be referred to as (cis)3'-dA₅₈-5'(trans); the system is shown in Fig. 7*b* *Inset*. In the second system, the 5' end was located at the cis side. The applied bias forced DNA strands toward the trans compartment. In Fig. 7*a*,

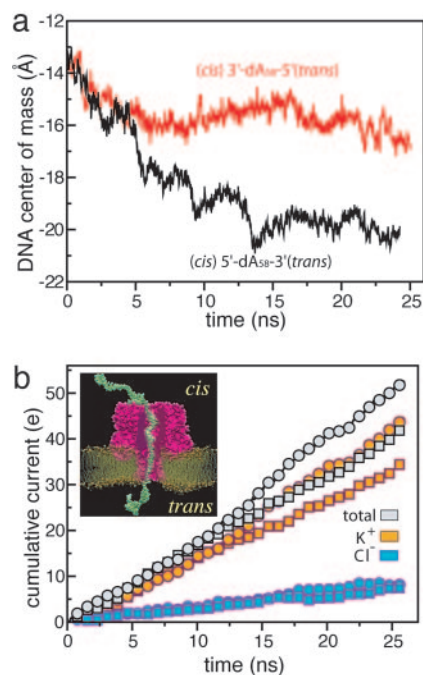


Fig. 7. MD simulation of DNA electrophoresis through the transmembrane pore of α -HL. (a) Center of mass of two sequence-wise identical but global orientation-wise different poly(dA₅₈) strands vs. time. Both strands translocate through the pore of α -HL driven by a 1.2-V bias. The poly(dA₅₈) strand is observed to move further toward the trans side with its 3' end forward. (b) Simulated cumulative currents of ions through the α -HL channel when it is blocked by two sequence-wise identical but global orientation-wise different poly(dA₅₈) strands. The global orientation of a DNA strand is characterized by the location of its 3' and 5' ends; (cis)5'-dA₅₈-3'(trans) data are plotted as squares, whereas (cis)3'-dA₅₈-5'(trans) data are plotted as circles. (*Inset*) A 356,065-atom microscopic model of the experimental system comprising of one α -HL channel (maroon), DPPC lipid bilayer (brown), a 58-nt DNA strand (lime), water, and ions (not shown).

we present how the DNA center of mass shifted through the pore over the duration of 25 ns. One clearly observes faster translocation for the DNA strand entering the pore 3' end first from the cis side, in agreement with the experimental results discussed earlier (HP3'). Visual inspection of the DNA translocation events with VMD (20) revealed the molecular mechanism for the directionality of the translocation kinetics. In the case of a field forcing ssDNA 3' end first through the pore, the bases remain tilted in the same (3'-to-5') direction; in the opposite orientation the bases have to reorient to fit through the pore at its narrow parts (see supporting information).

We further computed the currents of K⁺ and Cl⁻ ions flowing through the α -HL during polynucleotide translocation according to the procedure described in ref. 19. In Fig. 7*b*, we plot, in unitary charge units ($e = 1.6 \times 10^{-19}$ C), the resulting cumulative currents. A linear regression fit yields the average total currents of 330 pA for (cis)5'-dA₅₈-3'(trans) and 280 pA for (cis)3'-dA₅₈-5'(trans), which are 24% and 20% of the open pore current, respectively (19). Although we cannot directly compare these values to measured currents, the ratio of the currents, which is 1.2, is close to the experimental value (1.3). We found that the total current is mostly generated by the flow of K⁺ ions; the ratio of K⁺ to Cl⁻ current at a 1.2-V bias is $\approx 5:1$. Inside the α -HL pore, the ions remain hydrated; their trajectories pass through volumes free of DNA. The total charge carried by K⁺ and Cl⁻ ions inside the α -HL stem remained constant (15 ± 1) in both simulations.

Discussion and Conclusions

Previous studies demonstrated that the voltage-driven translocation dynamics of single-stranded DNA and RNA through the α -HL pore is dominated by the nucleic acid–pore interactions (4, 5, 13–15). Here, we have extended these studies to address the influence of DNA orientation on the translocation dynamics. Our experiments unambiguously demonstrate that threading single-stranded DNA from its 3' end through the pore is different from 5' threading: First, the residual ion current is lower for the 3' entries from the cis side of the pore versus 5' entries (9% versus 12%, respectively, of the open pore current); and, second, the sliding dynamics of the polynucleotide from the pore under applied voltage, or at zero voltage, is highly sensitive to the DNA orientation. Voltage-driven 3' entries from the cis side of the pore are faster than the corresponding 5' entries, and going in the reverse way (escape from the pore to the cis side after full threading) is slower for the 3' end as compared with the 5'.

The existence of two ion current states, which are highly correlated with the orientation of the polynucleotides (Fig. 2), indicates that molecules entering from the 3' end interact differently with the pore from those threaded with the 5' end. These results agree well with an extensive all-atom MD simulations, which take into account the asymmetric DNA and pore degrees of freedom, as well as ion and water molecules: (i) The ion current flowing through the blocked pore is larger for a 5'-end-threaded DNA (entered from cis) as compared with the 3'-threaded molecule, by 20%. The MD simulations (Fig. 7b) suggest that the current is mostly carried by the K⁺ ions in agreement with ref. 21. (ii) The DNA escape from the pore depends on its orientation, in the manner that the experiments suggest. The MD simulations provide a microscopic mechanism for the different interactions of the 3'-threaded DNA versus the 5' DNA with the pore. ssDNA, confined in a pore, straightens its backbone from an initial helical shape and as a result tilts its bases toward the 5' end, yielding a highly asymmetric structure.

While the MD simulations provide insight on the underlying microscopic short time behavior of the system, the DNA escape measurements reflect thousands of random walk steps, which is the long time limit of our system. The extrapolation from the short time to the long time behavior is not simple. Here, we use the general formalism described in ref. 14 to compute an effective, long-time diffusion constant for the DNA escape experiment, Fig. 3. A slight modification in the boundary conditions used in ref. 14 (to account for the hairpins) can be made to calculate the derivative of the escape probability density

function of our DNA hairpins, $P'(y)$ (see supporting information for complete derivation). We obtain

$$P'(y) = \pi/2 \sum_{m=0}^{\infty} (4m+1)e^{-\frac{\pi^2}{8}y(4m+1)^2} - (4m+3)e^{-\frac{\pi^2}{8}y(4m+3)^2}, \quad [1]$$

with $y = 2Dt_{\text{off}}/L^2$, where D is an effective 1D diffusion constant of the DNA, and L is the length of the single-stranded overhang in our experiment. Eq. 1 can be readily integrated for any given t_{off} value to yield the escape probability $P(y)$, or the stay probability, $1 - P(y)$, shown in Fig. 3. We used this function to fit our data for $t_{\text{off}} > 100 \mu\text{s}$ (dashed lines). From these fits, we can calculate the diffusion constants $D = 3.06 \times 10^{-10}$ and $1.77 \times 10^{-10} \text{ cm}^2/\text{s}$ for HP5' and HP3', respectively. For small assisting voltages, the polymer mobility μ must be related to the diffusion constant by an Einstein relation $\mu = D/k_B T$ (14). Thus, the different diffusion constants cited above imply immediately that HP5' will retract faster than HP3' when the assisting voltage is small, consistent with Fig. 5. Using the two diffusion constant values and the fast escape time scale of molecules from the pore, we can also obtain an estimate for the number of nucleotides, N' , that are associated with the fast processes ($t_{\text{off}} < 100 \mu\text{s}$) due to partial entry of the DNA in the pore. We obtain $N' \sim 4$ nucleotides. Note, however, that our data does not permit an accurate determination of D for $t_{\text{off}} < 100 \mu\text{s}$, and thus N' is most likely > 4 .

In conclusion, our results clearly demonstrate that the interaction potential between ssDNA and the α -HL protein pore strongly depends on the orientation of the threaded nucleotides, leading to an ≈ 2 -fold difference in the DNA dynamics. We have characterized experimentally the two fundamental diffusion constants associated with 3' and 5' ssDNA sliding. Moreover, the two DNA orientations give rise to different ion current blockades, in agreement with previous measurements (7). MD simulations of our system predicted a similar asymmetry and elucidated the molecular basis of the asymmetry by revealing a base tilt mechanism. Our work underlines a structural mechanism for the asymmetric interactions of the ssDNA inside a confining proteinic environment, which could be highly relevant to other motor proteins–DNA systems, such as helicases.

We thank H. Visram for assistance in data collection; M. Bates for contribution in the initial phase of the project; and A. Grosberg, H. Diamant, A. Ajdari, and M. Burns for stimulating discussions. A.M. and D.R.N. were supported by National Science Foundation Grant 0403891. A.A. and K.S. were supported by National Institutes of Health Grant P41 RR05969. Supercomputer time was provided to A.A. and K.S. by National Resource Allocation Committee Grant MCA93S028.

- Simon, S. M., Peskin, C. S. & Oster, G. F. (1992) *Proc. Natl. Acad. Sci. USA* **89**, 3770–3774.
- Driselkelmann, B. (1994) *Microbiol. Rev.* **58**, 293–316.
- Kasianowicz, J. J., Brandin, E., Branton, D. & Deamer, D. (1996) *Proc. Natl. Acad. Sci. USA* **93**, 13770–13773.
- Akeson, M., Branton, D., Kasianowicz, J., Brandin, E. & Deamer, D. (1999) *Biophys. J.* **77**, 3227–3233.
- Meller, A., Nivon, L., Brandin, E., Golovchenko, J. & Branton, D. (2000) *Proc. Natl. Acad. Sci. USA* **97**, 1079–1084.
- Howorka, S., Movileanu, L., Braha, O. & Bayley, H. (2001) *Proc. Natl. Acad. Sci. USA* **98**, 12996–13001.
- Wang, H., Dunning, J. E., Huang, A. P.-H., Nyamwanda, J. A. & Branton, D. (2004) *Proc. Natl. Acad. Sci. USA* **101**, 13472–13477.
- Song, L., Hobaugh, M., Shustak, C., Cheley, S., Bayley, H. & Gouaux, J. (1996) *Science* **274**, 1859–1865.
- Meller, A. & Branton, D. (2002) *Electrophoresis* **23**, 2583–2591.
- Vercoutere, W. A., Winters-Hilt, S., Olsen, H., Deamer, D., Haussler, D. & Akeson, M. (2001) *Nat. Biotechnol.* **19**, 248–252.
- Sauer-Budge, A. F., Nyamwanda, J. A., Lubensky, D. K. & Branton, D. (2003) *Phys. Rev. Lett.* **90**, 238101.
- Mathé, J., Visram, H., Viasnoff, V., Rabin, Y. & Meller, A. (2004) *Biophys. J.* **87**, 3205–3212.
- Bates, M., Burns, M. & Meller, A. (2003) *Biophys. J.* **84**, 2366–2372.
- Lubensky, D. & Nelson, D. (1999) *Biophys. J.* **77**, 1824–1838.
- Meller, A., Nivon, L. & Branton, D. (2001) *Phys. Rev. Lett.* **86**, 3435–3438.
- Kalé, L., Skeel, R., Bhandarkar, M., Brunner, R., Guroy, A., Krawetz, N., Phillips, J., Shinozaki, A., Varadarajan, K. & Schulten, K. (1999) *J. Comp. Phys.* **151**, 283–312.
- Cornell, W. D., Cieplak, P., Bayly, C. I., Gould, I. R., Merz, K. M., Jr., Ferguson, D. M., Spellmeyer, D. C., Fox, T., Caldwell, J. W. & Kollman, P. A. (1995) *J. Am. Chem. Soc.* **117**, 5179–5197.
- MacKerell, A. D., Jr., Bashford, D., Bellott, M., Dunbrack, R. L., Jr., Evanseck, J., Field, M. J., Fischer, S., Gao, J., Guo, H., Ha, S., et al. (1998) *J. Phys. Chem. B* **102**, 3586–3616.
- Aksimentiev, A. & Schulten, K. (2005) *Biophys. J.* **88**, 3745–3761.
- Humphrey, W., Dalke, A. & Schulten, K. (1996) *J. Mol. Graphics* **14**, 33–38.
- Sanchez-Quesada, J., Saghatelian, A., Cheley, S., Bayley, H. & Ghadiri, M. (2004) *Angew. Chem. Int. Ed.* **43**, 3063–3067.